

Moment Algorithms for Blood Vessel Detection in Infrared Images of Laser-Heated Skin

S. Shoari, N. Bagherzadeh

University of California

Dept. of Elec. and Computer Engineering
Irvine, CA

T. E. Milner, J. S. Nelson

University of California

Beckman Laser Inst. and Medical Clinic
Irvine, CA

Abstract

Block-detection and three-dimensional moment algorithms are applied to determine the presence and orientation of cylinders in a three-dimensional image. The proposed method detects blood vessels in a three-dimensional tomographic image constructed by infrared radiometry. Based on the moment principle, the method can be employed to determine the centroid, diameter, and orientation of arbitrarily shaped blood vessels for application in the laser treatment of hypervascular skin lesions.

Key Words: Block detection, blood vessel, image processing, infrared image, three-dimensional moments.

1 Introduction

Successful laser treatment of hypervascular lesions is based on proper selection of the irradiation parameters [3, 14, 16]. Kimel et al. [11], and Nelson et al. [17] have shown laser pulse duration should approximately equal the *thermal relaxation time*, τ_r , of the targeted blood vessels.

Three dimensional reconstruction of laser heated discrete subsurface chromophores in human skin recorded by infrared imaging radiometry is being investigated to determine the initial space dependent temperature distribution in skin to pulsed laser exposure [4, 7]. By imaging the emitted radiation onto an infrared focal plane array, useful information regarding the laser irradiated skin can be derived [15]. The value of τ_r is directly proportional to the squared diameter (d) of the target blood vessel

and inversely proportional to *thermal diffusivity* of skin, $\tau_r = d^2/16\chi$, where χ is thermal diffusivity and governs the rate of diffusive heat propagation in the material ($1.1 * 10^{-3} cm^2/s$) [5].

We model a blood vessel as a cylinder and use the block-detection and three-dimensional moment algorithms to estimate centroid, diameter, and orientation. This information is important for proper selection of laser pulse duration. Results presented here combined with access to lasers with user-specified pulse durations (0.25-15 ms) may provide a methodology for improved PWS (Port Wine Stains) treatment.

In Section 2, moments for blood vessel detection and their properties are described. Algorithms for block detection and three-dimensional moment calculation are given in Section 3. Experimental results and conclusions are given in sections 4 and 5, respectively.

2 Moments

To detect a pattern in an image, an invariant feature is selected independent of size, position, and orientation [8, 9, 10, 12, 18, 19, 13]. The mathematical foundation of an invariant feature is based on calculus of algebraic invariants [6]. Hu [9] has derived results showing the algebraic invariant of two-dimensional moments. Alt [2] applied these results for the recognition of letters and numerals. Kavianpour et al. [10] considered ellipse detection by moments. Dudani et al. [8] have applied moment invariants to identify aircraft. Abu-Mostafa and Psatlis [1] introduced the notion of complex moments and derived various invariants. Sadjadi and Hall [18], Lo and Don [12] have considered the extension of the moment invariant from two- to three-dimensions.

2.1 Three-dimensional Moments

Given an object with a three-dimensional density function, $f(x, y, z)$, the $(p+q+r)th$ order moments are defined in terms of a Riemann integral as:

$$m_{pqr} = \int_{-\infty}^{+\infty} \int_{-\infty}^{+\infty} \int_{-\infty}^{+\infty} r_x^p r_y^q r_z^r f(x, y, z) dx dy dz \quad (1)$$

where r_i is the normal distance to axis i , $i = x, y, z$, and $p, q, r = 0, 1, 2, \dots$. The integration extends over domain of f .

For an object with a finite extent (i.e., bounded domain), the integration extends over the object volume. The second order moments [e.g., ($p = 2, q = 0, r = 0$) *moment of inertia*] about x, y , and z axes are:

$$m_{200} = \int_{-\infty}^{+\infty} \int_{-\infty}^{+\infty} \int_{-\infty}^{+\infty} (y^2 + z^2) f(x, y, z) dx dy dz$$

$$m_{020} = \int_{-\infty}^{+\infty} \int_{-\infty}^{+\infty} \int_{-\infty}^{+\infty} (x^2 + z^2) f(x, y, z) dx dy dz$$

$$m_{002} = \int_{-\infty}^{+\infty} \int_{-\infty}^{+\infty} \int_{-\infty}^{+\infty} (x^2 + y^2) f(x, y, z) dx dy dz$$

where $r_x^2 = y^2 + z^2$, $r_y^2 = x^2 + z^2$, and $r_z^2 = x^2 + y^2$.

Definition 1: An object *centroid* is defined by coordinates \bar{x} , \bar{y} , and \bar{z} given by: $\bar{x} = m_{100}/m_{000}$, $\bar{y} = m_{010}/m_{000}$, and $\bar{z} = m_{001}/m_{000}$, where m_{000} is the object volume.

Central object moments with density function $f(x, y, z)$ are defined as:

$$\mu_{pqr} = \int_{-\infty}^{+\infty} \int_{-\infty}^{+\infty} \int_{-\infty}^{+\infty} (x - \bar{x})^p (y - \bar{y})^q (z - \bar{z})^r f(x, y, z) dx dy dz$$

A uniqueness theorem states that if $f(x, y, z)$ is piecewise continuous and bounded in a finite region in R^3 space, then moments of all order exist implying that the application of a small set of low-order moments may be used to distinguish different patterns.

We consider binary images so that $f(x, y, z)$ is either 0 or 1.

In a three-dimensional image, x, y , and z correspond to row (first dimension), column (second dimension), and frame (third dimension) of the voxel, respectively. One representation of a digital image is a collection of voxels with associated intensity values. For industrial applications, region segmentation or edge detection are used to transform images into a binary representation, where each voxel is either 0 (white) or 1 (black). Eq.(1) is written as a summation, and the $(p + q + r)^{th}$ order moment of a three-dimensional image with n rows, m columns, and l frames is:

$$m_{pqr} = \sum_{i=1}^n \sum_{j=1}^m \sum_{k=1}^l x_{ijk}^p y_{ijk}^q z_{ijk}^r \quad (2)$$

Here x_{ijk} , y_{ijk} , and z_{ijk} are the black pixel coordinates, and $m \cdot n \cdot l$ is the total number of voxels.

Similarly, central moments of a three-dimensional binary image are:

$$\mu_{pqr} = \sum_{i=1}^n \sum_{j=1}^m \sum_{k=1}^l (x_{ijk} - \bar{x})^p (y_{ijk} - \bar{y})^q (z_{ijk} - \bar{z})^r$$

3 Cylinder Detection Algorithms

In this section, algorithms for detecting the presence, diameter, and orientation of a cylindrical object in a three-dimensional image are presented.

3.1 Block-detection Algorithm

An algorithm for detecting connected black pixels in an $n \times m$ binary image is described.

Connectivity among pixels can be defined in terms of their adjacency. Figure 1 illustrates a pixel with eight neighbors.

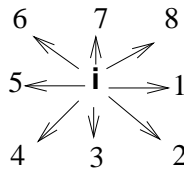


Figure 1: A pixel with neighbors

Two black pixels (x_1, y_1) and (x_2, y_2) are an 8-neighbor if:

$$\max\{|x_1 - x_2|, |y_1 - y_2|\} \leq 1$$

and 4-neighbor if:

$$\{|x_1 - x_2| + |y_1 - y_2|\} \leq 1$$

Two black pixels (x_1, y_1) and (x_k, y_k) are said to be connected by 8-path (4-path) if there exists a sequence of black pixels (x_p, y_p) , $2 \leq p \leq k$, such that each pair of pixels (x_{p-1}, y_{p-1}) and (x_p, y_p) are 8-neighbors (4-neighbors). In this paper we use 8-neighbors.

Since a three-dimensional image has blocks in different frames of the image, a block-detection algorithm identifies three-dimensional blocks.

3.2 Cylinder Centroid

Figure 2 illustrates a cylinder with minor, intermediate, and major axes along x , y , and z , respectively.

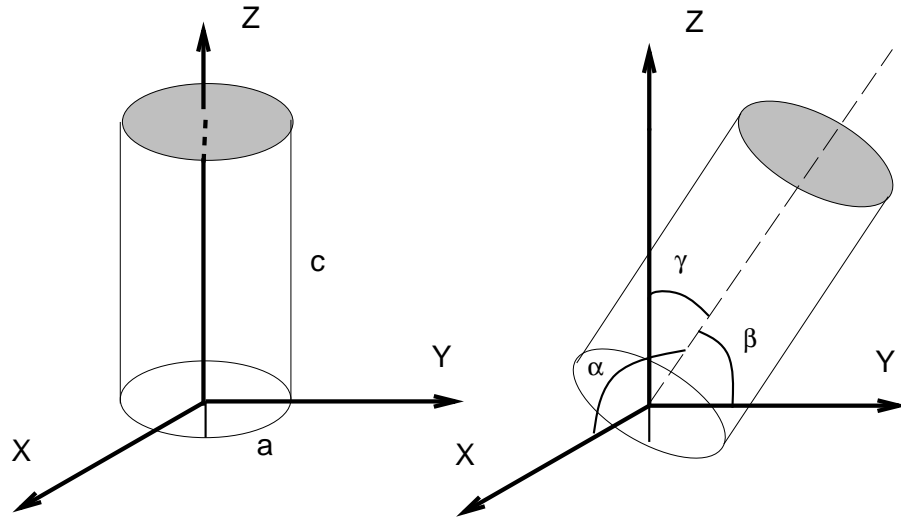


Figure 2: Cylinder geometry

For a cylinder $m_{000} = V = \pi a^2 c$, where V is the volume,

$$m_{001} = 4 \int_0^c \int_0^a \int_0^{\sqrt{a^2-y^2}} z dx dy dz = \frac{\pi a^2 c^2}{2}$$

Since $m_{100} = m_{010} = 0$, the centroid is at $(0, 0, \frac{c}{2})$.

If a given block image contains $n \times m \times l$ voxels, the $(p + q + r)^{th}$ order moment are calculated [Eq.(2)], and the centroid coordinates are:

$$\bar{x} = m_{100}/m_{000}, \bar{y} = m_{010}/m_{000}, \text{ and } \bar{z} = m_{001}/m_{000}. \quad (3)$$

where m_{000} represents the total number of black voxels in all frames of a block.

3.3 Algorithms for Calculating Cylinder Diameter and Orientation

In this section, algorithms to calculate cylinder orientation and diameter in a three-dimensional image are presented. An important cylinder property is described in Lemma 1.

Lemma 1: In a cylinder with $\frac{x^2}{a^2} + \frac{y^2}{a^2} = 1$, $0 \leq z \leq c$ and $a < c$, the second moment is minimum along the major axis and maximum along the minor axis; these moments are given by,

$$m_{002} = V\left(\frac{a^2}{2}\right) \text{ and } m_{200} = m_{020} = V\left(\frac{a^2}{4} + \frac{c^2}{3}\right) \quad (4)$$

Proof: The second moment, with respect to the $x - y$ plane, m_{xy} , is calculated as:

$$m_{xy} = \int_0^c z^2 dz \int_0^a dx \int_0^{\sqrt{a^2-x^2}} dy = \int_0^c (\pi a^2) z^2 dz = \frac{\pi a^2 c^3}{3} = V \frac{c^2}{3}$$

where $V = \pi a^2 c$ is the cylinder volume.

Similarly, moments with respect to $y - z$ and $x - z$ planes are:

$$m_{xz} = 4 \int_0^c dz \int_0^a dx \int_0^{\sqrt{a^2-x^2}} y^2 dy = \frac{4c}{3} \int_0^a \sqrt{(a^2-x^2)^3} dx$$

Using $x = a \sin \theta$ and $dx = a \cos \theta d\theta$:

$$m_{xz} = \frac{4a^4 c}{3} \int_0^{\frac{\pi}{2}} \cos^4 \theta d\theta = \frac{\pi c a^4}{4} = V \frac{a^2}{4}$$

Similarly, $m_{yz} = V \frac{a^2}{4}$

The second moment m_{200} for a cylindrical object about the x -axis is the sum of moments about $x - z$ and $x - y$ planes:

$$m_{200} = \int_{-\infty}^{+\infty} \int_{-\infty}^{+\infty} \int_{-\infty}^{+\infty} (y^2 + z^2) dx dy dz = m_{xz} + m_{xy}$$

$$m_{200} = V\left(\frac{a^2}{4} + \frac{c^2}{3}\right)$$

Similarly, m_{020} and m_{002} are given by:

$$m_{020} = V\left(\frac{a^2}{4} + \frac{c^2}{3}\right), \quad m_{002} = V\left(\frac{a^2}{4} + \frac{a^2}{4}\right) = V\left(\frac{a^2}{2}\right).$$

With the assumption that $a < c$, then $m_{002} < m_{200}$.

For a cylinder $m_{110} = m_{101} = m_{011} = 0$.

Definition 2: The angles between minor, intermediate, and major cylinder axes and positive direction of the x , y , and z axes, α , β , and γ , are defined as the cylinder *orientation* with respect to a given coordinate system (Figure 2).

The following three-dimensional second order moments J_1 , J_2 , and $|J_3|$ are invariants [18].

$$J_1 = \mu_{200} + \mu_{020} + \mu_{002}$$

$$J_2 = \mu_{020}\mu_{002} - \mu_{011}^2 + \mu_{200}\mu_{002} - \mu_{101}^2 + \mu_{200}\mu_{020} - \mu_{110}^2$$

$$|J_3| = \det \begin{bmatrix} \mu_{200} & \mu_{110} & \mu_{101} \\ \mu_{110} & \mu_{020} & \mu_{011} \\ \mu_{101} & \mu_{011} & \mu_{002} \end{bmatrix}$$

The second moment $|J_3|$ is invariant under rotation. Orientation R is given as:

$$R = \begin{bmatrix} r_1 \\ r_2 \\ r_3 \end{bmatrix} = \begin{bmatrix} \cos \alpha \\ \cos \beta \\ \cos \gamma \end{bmatrix}$$

The cylinder orientation in terms of different order moments can be calculated. The direction R can be found by determining the *eigenvector* corresponding to the minimum eigenvalue which represents the central moment along the major axis of the cylinder.

$$J_3 - \lambda I = \begin{bmatrix} \mu_{200} - \lambda & \mu_{110} & \mu_{101} \\ \mu_{110} & \mu_{020} - \lambda & \mu_{011} \\ \mu_{101} & \mu_{011} & \mu_{002} - \lambda \end{bmatrix}$$

Eigenvalues (λ) of J_3 are determined by solving the *characteristic equation*:

$$|J_3 - \lambda I| = f(\lambda) = \lambda^3 - J_1\lambda^2 + J_2\lambda - |J_3| \quad (5)$$

Where I is a diagonal unit matrix.

By assuming that a coordinate system originating at the centroid, where the z -axis is coincident with the major axis of the cylinder, the roots of the characteristic equation are:

$$\lambda_1 = V\left(\frac{a^2}{4} + \frac{c^2}{3}\right)$$

$$\lambda_2 = V\left(\frac{a^2}{4} + \frac{c^2}{3}\right)$$

$$\lambda_3 = V\left(\frac{a^2}{2}\right)$$

In this configuration, moments and central moments are equal, and roots of the characteristic equation are the second moments as given in Lemma 1 [Eq.(4)].

Solving for a and c :

$$\begin{aligned} a &= \sqrt{\frac{2\lambda_3}{V}} \\ c &= \sqrt{\frac{\frac{3}{2}(2\lambda_1 - \lambda_3)}{V}} \end{aligned} \quad (6)$$

Where $2a$ is the diameter and c is the length of the cylinder. The eigenvector R corresponding to the minimum eigenvalue (λ_3) gives the orientation of the cylindrical object. To determine the eigenvector corresponding to λ_3 , a set of homogeneous linear equations is solved:

$$\begin{bmatrix} \mu_{200} - \lambda_3 & \mu_{110} & \mu_{101} \\ \mu_{110} & \mu_{020} - \lambda_3 & \mu_{011} \\ \mu_{101} & \mu_{011} & \mu_{002} - \lambda_3 \end{bmatrix} \begin{bmatrix} r_1 \\ r_2 \\ r_3 \end{bmatrix} = 0 \quad (7)$$

$$\begin{aligned} r_1 &= (\mu_{020} - \lambda_3)(\mu_{002} - \lambda_3) - \mu_{101}(\mu_{020} - \lambda_3) - \mu_{110}(\mu_{002} - \lambda_3) + \mu_{011}(\mu_{101} + \mu_{110} - \mu_{011}) \\ r_2 &= (\mu_{002} - \lambda_3)(\mu_{200} - \lambda_3) - \mu_{110}(\mu_{002} - \lambda_3) - \mu_{011}(\mu_{200} - \lambda_3) + \mu_{101}(\mu_{110} + \mu_{011} - \mu_{101}) \\ r_3 &= (\mu_{200} - \lambda_3)(\mu_{020} - \lambda_3) - \mu_{011}(\mu_{200} - \lambda_3) - \mu_{101}(\mu_{020} - \lambda_3) + \mu_{110}(\mu_{011} + \mu_{101} - \mu_{110}) \end{aligned}$$

4 Experimental Results on Blood Vessel Detection

Infrared imaging radiometry uses a high speed infrared focal plane array (IR-FPA) camera to measure temperature changes induced in human skin exposed to pulsed laser radiation. In practice, a pulsed laser is used to produce transient heating of the object under study (Figure 3). Heat generated due to light absorption by subsurface blood vessels in skin diffuses to the surface and results in increased infrared emission levels which is measured by a fast IR-FPA. If a pulsed laser source is used to irradiate the skin, an immediate increase in infrared emission will occur due to optical absorption by hemoglobin contained within the blood vessels. The infrared signals collected by each detector element are digitized by a 5 MHz, 12-bit A/D converter giving a frame rate of 217 HZ. An infrared imaging radiometry record of skin in response to pulsed laser exposure is composed of sequence of 150 gray-level frames (128×128) which are stored and accessed using a computer.

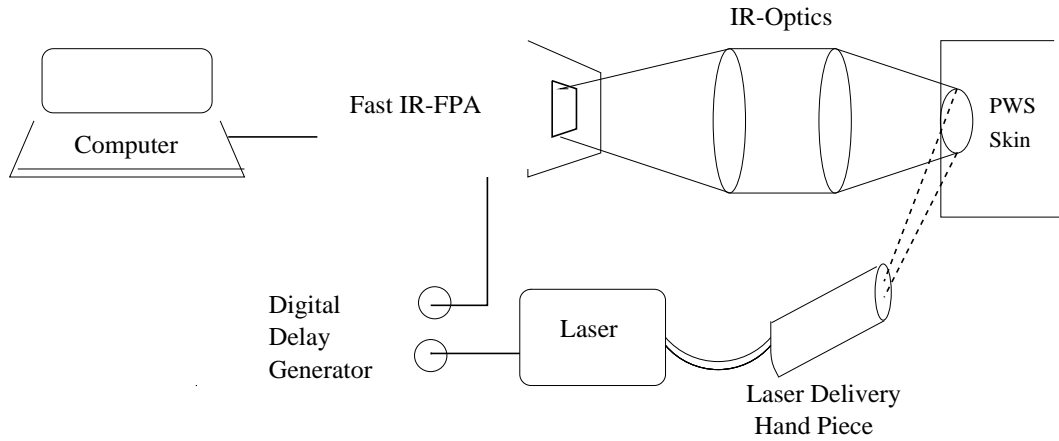


Figure 3: Infrared radiometry instrumentation

4.1 Processing Program

Commercial software [Application Visualization System (AVS), Waltham, MA] is used to process input images. Figure 4 illustrates Frame 1 of the input image. Dark pixels represent the blood vessels.

Each gray-level image undergoes a binary transformation using a threshold set at 85% of the average pixel value for each frame. The threshold was calculated using the background level. Figure 5 shows frame 1 after the gray-scale to binary transformation where numeral one represents a *black* voxel.

4.1.1 Block-detection Algorithm

Simulation programs for detecting blocks and calculating moments are written in C programming language. Figures 6, 7, and 8 represent blocks detected by the block-detection algorithm in frames 1, 3, and 5, respectively.

4.1.2 Blood Vessel Centroid

A time sequence of infrared emission frames may be viewed as a three-dimensional image, and moments can be applied to calculate the blood vessel centroid detected by the block detection algorithm. Table 1 lists the centroid coordinates of the first 15 blocks calculated using Eq.(3).

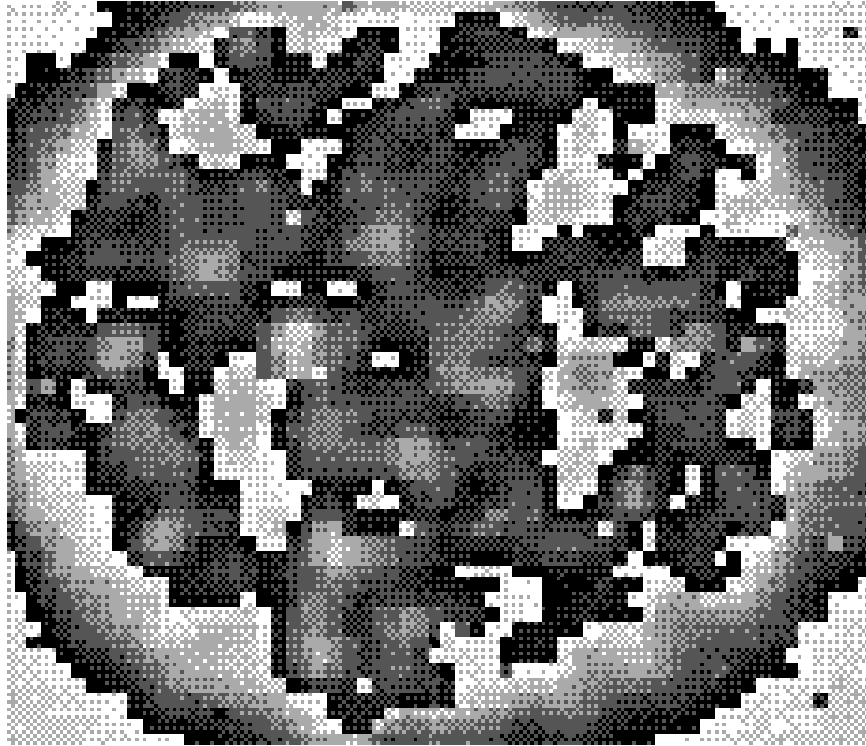


Figure 4: 128x128 voxels in Frame 1 of raw input image

4.1.3 Diameter and Orientation of Blood Vessels

In the analysis of input image, roots of the characteristic equation [Eq.(5)] were determined and used to calculate the diameter of blood vessels [Eq.(6)]. Table 2 illustrates the diameter (in pixels) of the first 15 detected blood vessels. Orientation for the same vessels is presented in Table 3.

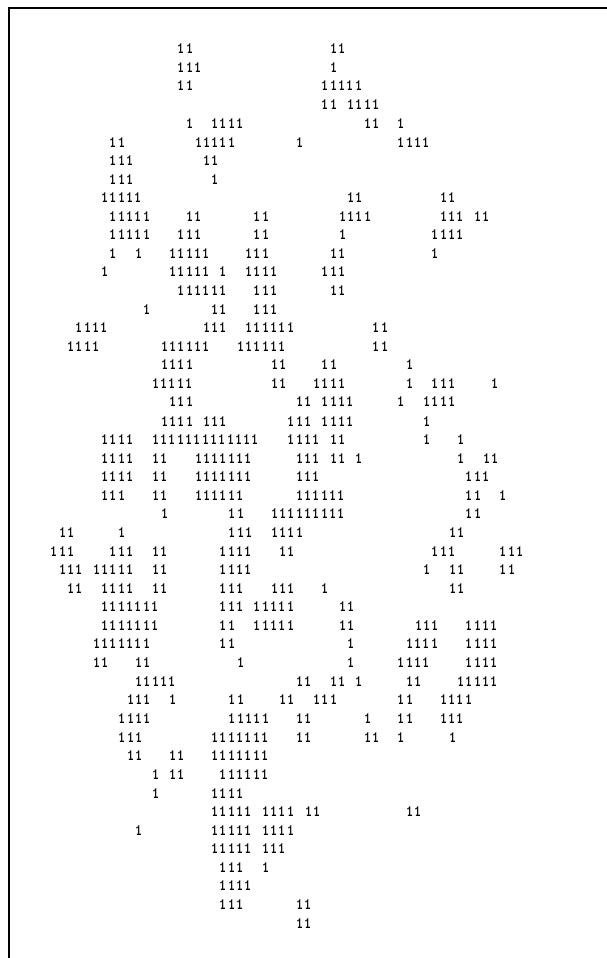


Figure 5: Frame 1 after transformation

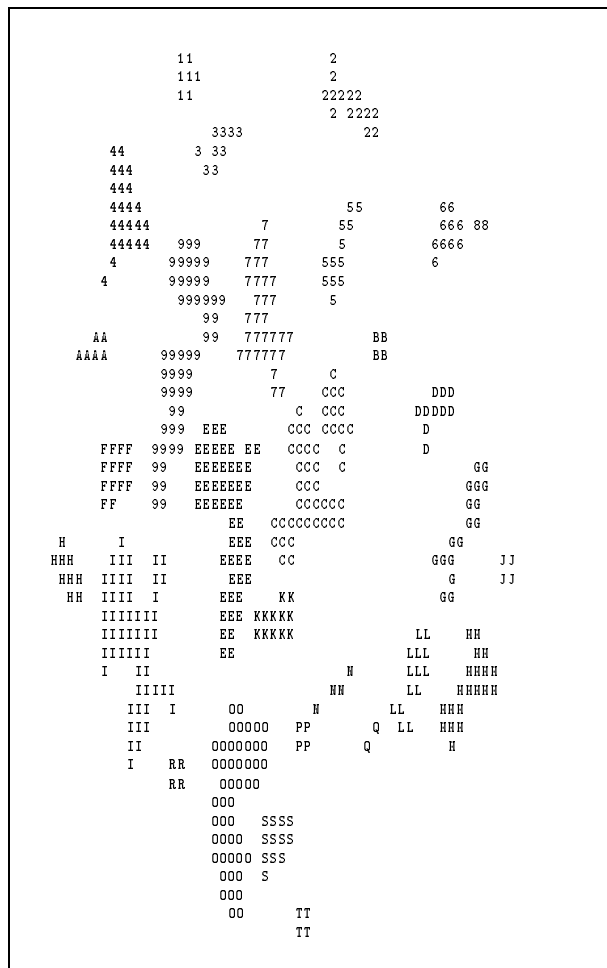


Figure 6: Blocks detected by the block-detection algorithm in Frame 1

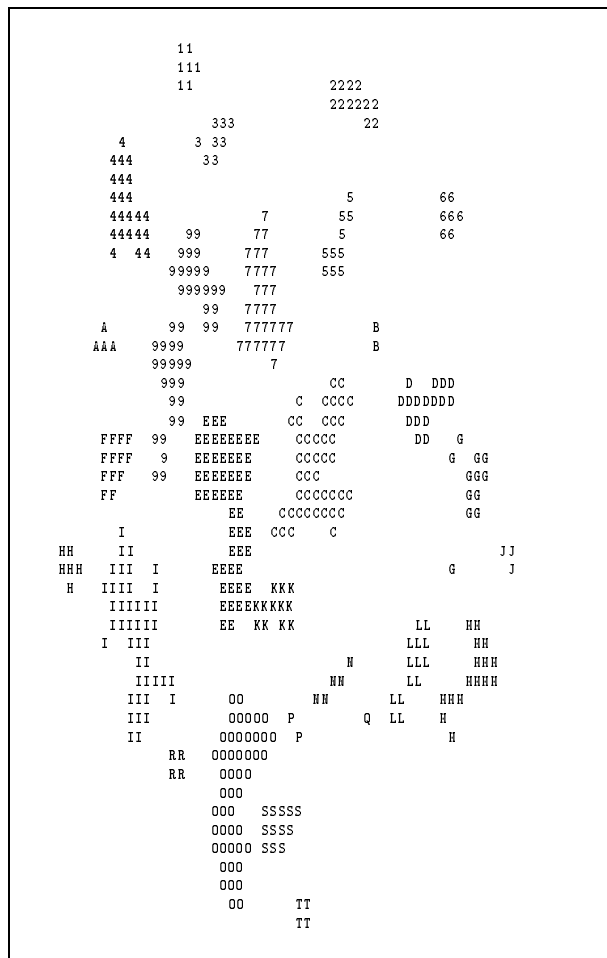


Figure 7: Blocks detected by the block-detection algorithm in Frame 3

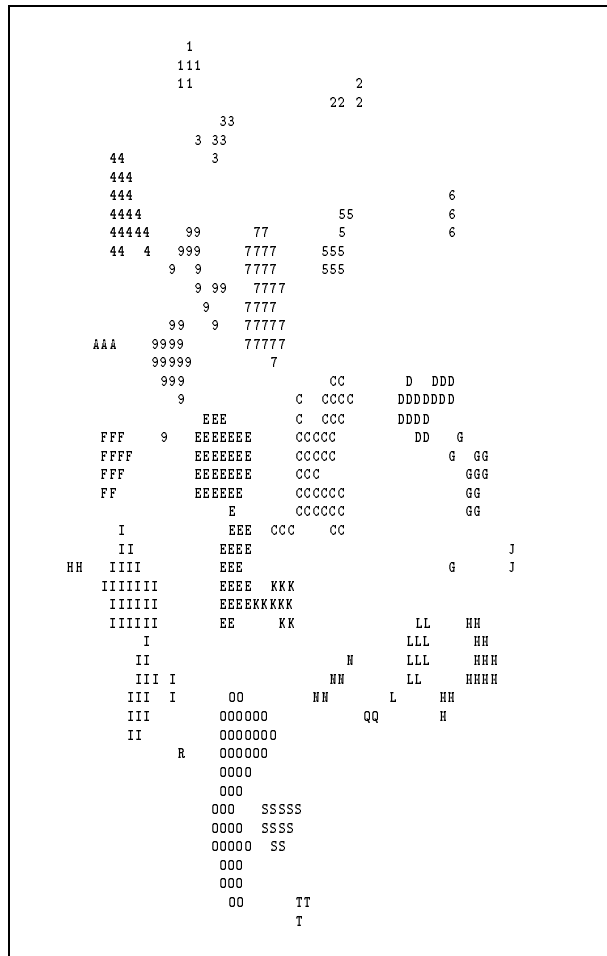


Figure 8: Blocks detected by the block-detection algorithm in Frame 5

<i>Block</i>	\bar{x}	\bar{y}	\bar{z}
B_1	4	17	5
B_2	5	37	2
B_3	7	21	3
B_4	12	10	7
B_5	13	35	5
B_6	12	48	3
B_7	17	27	10
B_8	12	52	1
B_9	18	15	23
B_A	18	7	3
B_B	18	40	1
B_C	25	34	25
B_D	22	45	9
B_E	27	23	24
B_F	26	9	23

Table 1: Centroids of detected blood vessels

<i>Block no.</i>	<i>Diameter</i>
B_1	2.6
B_2	5.0
B_3	3.9
B_4	5.7
B_5	4.1
B_6	3.0
B_7	6.0
B_8	1.6
B_9	8.3
B_A	2.6
B_B	1.8
B_C	8.4
B_D	5.6
B_E	10.1
B_F	3.6

Table 2: Diameter of detected blood vessels

<i>Block no.</i>	$\cos \alpha$	$\cos \beta$	$\cos \gamma$
B_1	0.604	0.732	0.341
B_2	0.586	0.722	0.368
B_3	0.487	0.687	0.538
B_4	0.514	0.712	0.420
B_5	0.624	0.727	0.478
B_6	0.549	0.722	0.420
B_7	0.514	0.712	0.478
B_8	0.487	0.687	0.538
B_9	0.604	0.720	0.340
B_A	0.606	0.721	0.336
B_B	0.608	0.722	0.328
B_C	0.612	0.723	0.317
B_D	0.617	0.725	0.303
B_E	0.624	0.727	0.283
B_F	0.624	0.727	0.283

Table 3: Orientation of detected blood vessels

5 Conclusion

Moments of a three-dimensional tomographic image constructed by infrared radiometry contain information which can be used to calculate the centroid, diameter, and orientation of individual blood vessels. Blood vessels, modeled as cylinders, are identified by a block-detection algorithm. Three-dimensional moment algorithms are used to compute diameter and orientation of blood vessels. This information may be important for proper selection of laser pulse duration for improved PWS treatment. Although the algorithms used images derived by infrared radiometry, this procedure can be implemented on images generated by other modalities (e.g., MRI). Results demonstrate the utility of the moment concept in medical image processing.

6 Acknowledgments

This work was supported by research grants awarded from the Biomedical Research Technology Program (R03-RR06988) and Institute of Arthritis and Musculoskeletal and Skin Diseases (1R29-AR41638-01A1 and 1R01-AR42437-01A1) at the National Institutes of Health, Whitaker Foundation (WF-9496) and Dermatology Foundation. Institutional support from the Office of Naval Research, Department of Energy, National Institutes of Health, and the Beckman Laser Institute and Medical Clinic Endowment is also gratefully acknowledged.

References

- [1] Y. S. Abu-Mostafa and D. Psatlis, "Recognitive Aspects of Moment Invariants," *IEEE Transaction on Pattern Analysis and Machine Intelligence* vol. 11, pp. 698-706, 1984.
- [2] F. Alt, "Digital Pattern Recognition by moments," *Optical Character Recognition* G.L. Fischer et al. Eds., Spartan, Washington, D.C., pp. 240-258, 1962.
- [3] M. W. Berns, "Laser Surgery," *Scientific American*, pp. 84-90, June 1991
- [4] S. Chaudhuri, S. Chatterjee, N. Katz, M. Nelson, and M. Goldbaum "Detection of Blood Vessels in Retinal Images Using Two-Dimensional Matched Filters," *IEEE Transactions on Medical Imaging* vol. 8, pp. 263-269, 1989

- [5] F. A. Duck, "Physical Properties of Tissue. A Comprehensive Reference Book", London, 1990
- [6] G. B. Gurevich, "Foundation of the Theory of Algebraic Invariants," *Noordhoff, Groningen* 1964.
- [7] D. Delaere, C. Smets, P. Suetens, G. Marchal, and F. Van de Werf "Knowledge-based System for the Three-dimensional Reconstruction of Blood Vessels from two Anangiographic Projections," *North Sea:Medical Physics and Imaging* pp. 27-36, 1991
- [8] S. A. Dudani, K. J. Breeding, and R. B. McGhee, "Aircraft Identification by Moment Invariants," *IEEE Transactions on Computers* C-26, pp. 39-45, 1977.
- [9] M. K. Hu, "Visual Pattern Recognition by Moment Invariants," *IRE Transactions in Information theory* IT-8, pp. 179-187, 1962.
- [10] A. Kavianpour, S. Shoari, and N. Bagherzadeh, "Ellipse Detection by Moments using a Pyramid Architecture" *International Journal of Computer and Electrical Eng.* vol. 21, no. 1, pp. 69-75, Jan. 1995
- [11] S. Kimel, L. O. Svaasand, M. H. Wilson, M. J. Schell, T. E. Milner, J. S. Nelson, and M. W. Berns "Differential Vascular Response to Laser Photothermolysis," *The Journal of Investigative Dermatology* vol. 103, no. 5, pp. 693-700, 1994
- [12] C. H. Lo and H. S. Don, "3-D Moment Forms: Their Construction and Application to object Identification and Positioning," *IEEE Transaction on Pattern Analysis and Machine Intelligence* vol. 11, no. 10, pp. 1053-1060, 1989.
- [13] L. M. Luo, X. H. Xie, X. D. Bao, and J. L. Coatrieux "Quantitative Detection of Blood Vessel Structures in MRI by Using 3-D Geometrical Moments," *Chinese Science Bulletin* vol. 39, pp. 785-789, 1994
- [14] T. E. Milner, D. M. Goodman, B. S. Tanenbaum, and J. S. Nelson "A Solution to Inverse Problem Associated with Pulsed Photothermal Radiometry," *JOSA A* , 1995
- [15] T. E. Milner, D. M. Goodman, B. S. Tanenbaum, B. Anvari, O. Svaasand, and J. S. Nelson "Imaging Laser Heated Subsurface Chromophores in Biological Materials: Determination of Lateral Physical Dimensions," *Phys. Med. Biol.* , vol.41, pp31-44, 1996

- [16] J. S. Nelson and M. W. Berns “Basic Laser Physics and Tissue Interactions,” *J. Contemporary Dermatology* vol. 2, no. 2, pp. 1-15, 1988.
- [17] J. S. Nelson and J. Applebaum “Clinical Management of Port-Wine Stain in Infants and Young Children Using Flashlamp-Pulsed Dye Laser,” *Clin. Pediatrics* vol. 29, pp. 503-508, 1990
- [18] F. A. Sadjadi and E. L. Hall, “Three Dimensional Moment Invariants,” *IEEE Transaction on Pattern Analysis and Machine Intelligence* vol. 2, pp. 127-136, 1980.
- [19] S. Shoari, A. Kavianpour, and N. Bagherzadeh, “Pyramid Simulation of Image Processing Applications” *Journal of Image and Vision Computing* vol. 12, no. 8, pp. 523-529, October 1994